JACS
JOURNAL OF THE AMERICAN CHEMICAL SOCIETY
Article
pubs.acs.org/JACS

# Gold Nanoparticles as Electronic Bridges for Laccase-Based Biocathodes

Cristina Gutiérrez-Sánchez,[†] Marcos Pita,*[,†] Cristina Vaz-Domínguez,[†,§] Sergey Shleev,[‡] and Antonio L. De Lacey*[,†]

[†]Instituto de Catalisis y Petroleoquimica, CSIC, c/Marie Curie 2, L10, 28049 Madrid, Spain

[‡]Biomedical Laboratory Science and Technology, Faculty of Health and Society, Malmo University, SE-205 06 Malmo, Sweden

Supporting Information

**ABSTRACT:** Direct electron transfer (DET) reactions between redox enzymes and electrodes can be maximized by oriented immobilization of the enzyme molecules onto an electroactive surface modified with functionalized gold nanoparticles (AuNPs). Here, we present such strategy for obtaining a DET-based laccase (Lc) cathode for $O_2$ electroreduction at low overpotentials. The stable nanostructured enzymatic electrode is based on the step-by-step covalent attachment of AuNPs and Lc molecules to porous graphite electrodes using the diazonium salt reduction strategy. Oriented immobilization of the enzyme molecules on adequately functionalized AuNPs allows establishing very fast DET with the electrode via their Cu T1 site. The measured electrocatalytic waves of $O_2$ reduction can be deconvoluted into two contributions. The one at lower overpotentials corresponds to immobilized Lc molecules that are efficiently wired by the AuNPs with a heterogeneous electron transfer rate constant $k_0 \gg 400\ s^{-1}$.

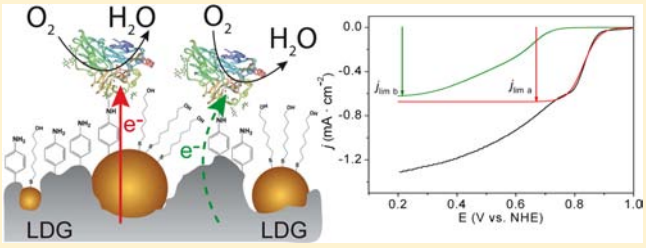


## INTRODUCTION

Bioelectrochemical systems have been a matter of constant ground-breaking research for the last decades.[1] In particular, a great effort has been directed toward studying the biocatalyzed interconversion of chemicals into electricity and vice versa for purposes such as amperometric biosensors development,[2] selective pollutant treatment,[3] or electrical power generation.[4] Redox enzymes are common biocatalysts used for these purposes, as it is possible to couple their enzymatic activity to electric current production when conveniently linked to an electrode.[5] There are two important factors for developing an efficient enzymatic electrode. The first one is optimizing the enzyme immobilization strategy in order to obtain a high coverage of active biocatalyst molecules on the electrode surface with high operational stability. The second one is establishing fast electron transfer between the redox sites of the immobilized enzyme molecules and the electrode. This electron transfer can be achieved by using redox mediators, which is known as mediated electron transfer (MET),[6] or by direct electron transfer (DET) between the enzyme redox centers and electrode.[5] DET has the advantage of avoiding the use of redox mediators, which complicate the enzyme electrode design, lead to higher overpotentials of the electrocatalytic process, reduce operational stability and frequently are toxic. On the other hand, DET requires a short distance (less than 15−20 Å) between the redox center of the immobilized enzyme and the electrode surface, which is not straightforward in many cases. Optimization of DET can be obtained by oriented immobilization of the enzyme molecules with their most exposed redox center facing the electrode surface.[7] Alternatively, DET can be greatly improved by modifying the electrode surface with conductive nanoelements, such as carbon nanotubes or gold nanoparticles (AuNPs). The similar size of these nanoelements and of enzymes, and the special physicochemical properties of the former facilitate their electronic coupling.[8] Moreover, the fabrication of nanostructured electrodes allows immobilizing a higher amount of the biocatalyst per geometric electrode area unit, and thus leading to higher catalytic current densities.[8d,9]

Laccases (Lc's) are one of the most interesting types of redox enzymes to be attached on electrodes because these multicopper oxidases are able to selectively catalyze $O_2$ reduction to $H_2O$ at low overpotential.[10] Therefore, they are good candidates for developing $O_2$-utilizing biocathodes for fuel cell applications. Lc's as other multicopper oxidases (MCO) have their Cu atoms grouped in two sites of the protein tridimensional structure. The T1 site contains one Cu ion and is the redox center of the Lc's that receives 4 electrons in 4 successive steps from the electron-donor substrate. The T2/T3 site contains 3 Cu ions and it is responsible of $O_2$ reduction to $H_2O$.[10]

MET-based Lc electrodes able to produce very high catalytic current densities of $O_2$ reduction have been reported, which are limited by the substrate transport rate to the electrode.[11] Currently, several research groups are doing a great effort in developing DET-based Lc's electrodes. The goal is to obtain such high catalytic currents as with MET-based electrodes, but decreasing the $O_2$ reduction overpotential while avoiding the

**Received:** July 25, 2012
**Published:** September 24, 2012

   dx.doi.org/10.1021/ja307308j | J. Am. Chem. Soc. 2012, 134, 17212−17220

other problems associated to the use of redox mediators. This requires that the reduction of $O_2$ by the Lc-modified electrode goes through the enzyme's Cu T1 site, not directly to the T2/T3 Cu site.[10a] For this purpose, several strategies of DET-based Lc's electrodes have been reported, either by oriented immobilization of the enzyme[12] or by its co-immobilization with conductive nanoelements.[13]

In the present work, we report a strategy for developing a DET-based Lc electrode that combines a nanostructured electrode and the enzyme oriented immobilization by tailor-made surface chemistry. We have covalently modified a porous carbon material, low density graphite (LDG), with AuNPs using an aromatic linker generated by electrochemical reduction of a diazonium salt.[14] Subsequently, the attached AuNPs were functionalized with a mixed monolayer of the aromatic diazonium derivative and a thiol for the covalent and oriented immobilization of *Trametes hirsuta* laccase (*Th*Lc) molecules. We show that this strategy allows designing robust nanostructured enzyme electrodes in which AuNPs act as electronic bridges between the redox sites of the enzyme molecules and the porous carbon electrode.

## MATERIALS AND METHODS

**Chemicals.** LDG rods of 3 mm diameter, $BF_4Bu_4N$, 4-nitrobenzene diazonium perchlorate, sodium nitrite, 1-(3-dimethylaminopropyl)-3-ethylcarbodiimide (EDC), 2,2′-azinobis-(3-ethylbenzothiazoline-6-sulfonic acid) diammonium salt (ABTS), sodium fluoride, *N*-hydroxysuccinimide (NHS), 6-mercapto-1-hexanol (MH), 30% $H_2O_2$, $NaIO_4$, $HAuCl_4$, tetrakis(hydroxymethyl)phosphonium chloride (THPC), and morpholino-ethanesulphonic acid (MES) were purchased from Sigma. NaOH, 98% $H_2SO_4$, absolute ethanol (EtOH), acetic acid 96%, sodium chloride, sodium *m*-peryodate and acetonitrile HPLC grade were purchased from Panreac. Acetonitrile was made anhydrous prior to use with molecular sieves (Sigma-Aldrich), whereas all other regents were used as received. All aqueous solutions were prepared with Milli Q (18.2 MΩ·cm) water.

**Enzymes.** *T. hirsuta* laccase (*Th*Lc) from the basidiomycete, strain *T. hirsuta* 56, was obtained from the laboratory collection of the Moscow State University of Engineering Ecology following the purification procedure previously reported.[15] The enzyme was homogeneous as judged from SDS-PAGE and HPLC. The highly concentrated preparations of *Th*Lc were stored in 0.1 M phosphate buffer, pH 6.5, at −20 °C. The concentration of the enzyme in stock solution was measured using BIO-RAD (Bio-Rad Laboratories) according to the Bradford method.[16] The calibration curve was done using bovine serum albumin (BSA) as the protein standard. The catalytic turnover of the enzyme was measured spectrophotometrically using 1 mM 2,2′-azinobis-(3-ethylbenzothiazoline-6-sulfonic acid) diammonium salt (ABTS) as substrate and its value was 397 $s^{-1}$, which is in good agreement with previously measured maximal catalytic constants of *Th*Lc toward different substrates.[15]

**Synthesis of Gold Nanoparticles.** Two sets of AuNPs were synthesized for further electrode modification. The first set comprised 5 ± 3 nm AuNPs freshly synthesized in aqueous media by addition of 1 mM $HAuCl_4$ to 60 mM NaOH solution containing 1 mM THPC under vigorous stirring.[17] The resulting AuNPs were filtered with a PTFE 0.200 μm pore size filter. For the second set of AuNPs, a solution of 38.8 mM of sodium citrate was prepared. A total of 125 mL of an $HAuCl_4$ 1 mM solution was heated to boil and 12.5 mL of citrate solution was added. Reactants were let to react for 15 min and let to cool down to room temperature.[18] The resulting AuNPs were 16 ± 2 nm in diameter. The AuNPs size in both preparations was determined by UV−vis spectroscopy using a numerical approximation method[19] and additionally confirmed by TEM microscopy.

**Preparation of Golden Nanostructures on Graphite Electrodes.** LDG or HOPG electrodes were cleaned, polished and modified with 4-aminophenyl groups as described by Vaz-Dominguez et al.[20] The modified electrodes were then immersed during 2 h in a 14.5 mM $NaNO_2$ and 0.5 M HCl solution in order to convert the aromatic amino groups of the electrode surface to diazonium groups. Subsequently, the electrodes were incubated into an aqueous dispersion of AuNPs during 3−72 h. Afterward, two cyclic voltammograms (CVs) were run between 0.6 and −0.6 V at 200 mV/s with the AuNP-LDG or AuNP-HOPG electrodes in 50 mM acetate buffer, pH 4.2, $NaClO_4$ 100 mM at room temperature.

**Immobilization of *T. hirsuta* Laccase.** The AuNP-LDG electrodes were immersed in an acetonitrile solution containing 2 mM *p*-nitrophenyldiazonium perchlorate and 100 mM $BF_4Bu_4N$. One CV from 0.6 V to −0.6 V with 200 mV/s scan rate was recorded. Afterward, the LDG electrodes were taken into a 9:1 $EtOH/H_2O$, 0.1 M KCl solution, and electrochemical reduction of the nitro groups on the LDG-AuNPs surface was carried out running a CV from 0 to −1.4 V at 200 mV/s scan rate. The amino-terminated LDG-AuNPs electrodes were then immersed overnight in a water solution containing 1 mM MH.

Five microliters of 7.5 mg/mL *Th*Lc solution was placed into 55 μL of 47 mM $NaIO_4$ solution for 30 min. Afterward, 90 μL of 100 mM $Na_2HPO_4$ was added to the solution. The modified AuNPs-LDG electrodes were then incubated in the *Th*Lc solution for 90 min. The *Th*Lc-AuNP-LDG electrodes were rinsed with 10 mM MES buffer, pH 6.0. Finally, the *Th*Lc-AuNP-LDG electrodes' surface was covered with 10 μL of 10 mM MES, pH 6.0, buffer solution containing 36 mM EDC and 17 mM NHS and tapped to avoid evaporation, letting the reaction take place for 2 h. Control *Th*Lc-LDG electrodes were prepared by covalent immobilization of the enzyme as just described on LDG electrodes functionalized with 4-aminophenyl groups.

**Electrochemical Measurements.** Electrochemical experiments were performed with an Autolab PGSTAT30 analyzer controlled by GPES 4.9 software (Eco Chemie, The Netherlands). Experiments were run in a three-electrode glass cell using a BAS Ag/AgCl reference electrode (204 mV vs NHE) and a platinum wire counter electrode. The cell temperature was controlled by a thermostatted water jacket. The LDG electrodes were connected to a MSR electrode rotator from Pine Instruments. Highly oriented pyrolytic graphite (HOPG) "edge" electrodes of 5 mm diameter were supplied by Pine Instruments. The HOPG electrodes were abraded with sandpaper and then polished successively with 1, 0.3, and 0.05 μm alumina slurries (Buehler) until the surface had a mirror-like appearance. Finally, the HOPG electrodes were sonicated in 1:2 ethanol/water for 10 min. The LDG electrodes were only abraded and sonicated. In the electrocatalytic measurements, current densities are reported relative to the geometric area of the electrodes and potentials are represented versus NHE for the sake of facilitating comparison with results from the literature.

**Transmission Electron Microscopy (TEM).** LDG electrodes at different modification stages were prepared for TEM analysis. The modified electrodes were abraded with sandpaper for 10 s. The resulting carbon chips were taken into an Eppendorf tube and filled with 500 μL of ethanol. The tubes were immersed into an ultrasound bath during 30 min. Twenty microliters of the gray solution was deposited on a Lacey Carbon Film on 200 mesh copper TEM grid (Electron Microscopy Sciences) and let dry. A 200 KV JEOL 2100 transmission electron microscope equipped with an Oxford Instruments EDX analyzer was used for the analyses.

**Mercury Porosimetry.** LDG disks of 3 mm diameter and 3 mm height were previously abraded with sandpaper and then degassed during 2 h under vacuum at 110 °C in order to eliminate adsorbed molecules. Hg intrusion porosimetry of the LDG disks was measured at 21 °C in a Poresizer 9320 (Micromeritics) porosimeter.

## RESULTS

**Preparation of AuNP-LDG Electrodes.** LDG is a very porous material with a high surface area. Hg intrusion porosimetry measurements indicated that the electrodes used in this work had a specific area of 5.4 $m^2/g$, 27% porosity and an average pore diameter of 5.5 μm, although pores in the 10−50 nm range were also detected (Figure S1, Supporting

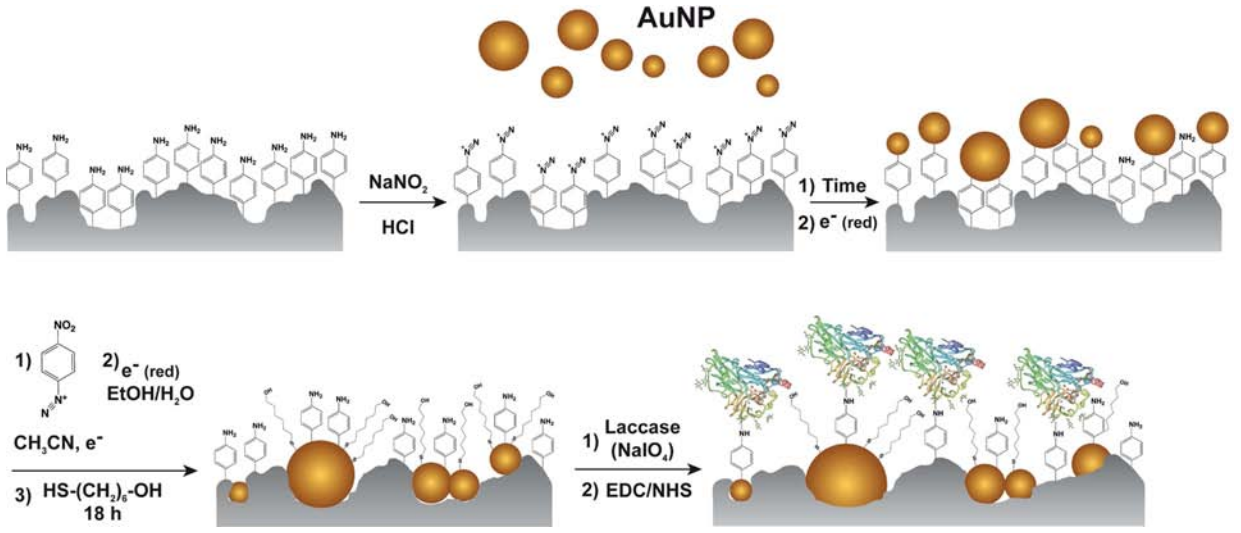


**Figure 1.** Scheme of the modification of LDG electrodes with AuNPs and *Th*Lc. Drawings are not at scale and only the chemical linkers formed at each step are shown. More than one layer of phenyl rings may be present in some regions of the LDG surface, although they are not represented for the sake of clarity.

Information). The porous surface of LDG electrodes has been shown to be a good platform for covalent immobilization of *Th*Lc and for measuring its electrocatalytic properties of $O_2$-reduction.[20] In this work, we have developed a strategy for attaching AuNPs to the LDG surface pores and subsequent *Th*Lc immobilization on the nanostructured electrode, in order to increase the rate of DET reactions.

The scheme of LDG electrodes modification with AuNPs and *Th*Lc molecules is shown in Figure 1. The formation a of a 4-aminophenyl layer on the LDG surface was performed as reported before.[20] The electrochemical parameters (number of voltammetric cycles and scan rate) for this modification step were selected to minimize formation of multiple layers on the electrode surface.[7b,9a,20] The CVs corresponding to the electrochemical reduction of *p*-nitrophenyldiazonium perchlorate and further electrochemical reduction of the grafted nitrophenyl groups are shown in the Supporting Information (Figure S2). The 4-aminophenyl groups of the electrode surface were then converted to diazonium groups by reaction with $NaNO_2$ in 0.5 M HCl (Figure 1). Afterward, the modified LDG electrodes were incubated in a AuNPs (5 nm) aqueous dispersion for different time periods so that the negatively charged AuNPs were electrostatically attracted to the positively charged electrode surface, diffusing through the LDG pores. Spontaneous reaction of the diazonium groups with the AuNPs takes place, forming Au−C covalent bonds.[21] After the incubation period, two CVs were run with the AuNPs-LDG electrodes aimed to ensure the covalent attachment of the AuNPs. The applied current caused the electrochemical reduction of the surface diazonium salts and allowed the formed phenyl radicals to react with the AuNPs. The first cycle shows the reduction wave of the diazonium groups at −0.2 V versus AglAgCll 3 M KCl (Figure S3, Supporting Information).

The presence of AuNPs immobilized on the graphite electrodes was confirmed by cyclic voltammetry in 0.1 M $H_2SO_4$.[22] To maximize the AuNPs coverage on the electrodes, its dependence on modification time was studied. This study was done with polished HOPG "edge" electrodes instead of LDG electrodes because the former have a much more reproducible electroactive area, therefore higher consistency was expected from the measurements. Figure 2A shows the CVs measured after different incubation times of modified HOPG electrodes, in which the typical redox signals of gold are observed. The intensity of the redox peaks increases with the incubation time in the AuNPs solution, indicating that more AuNPs were immobilized on the LDG surface. The total

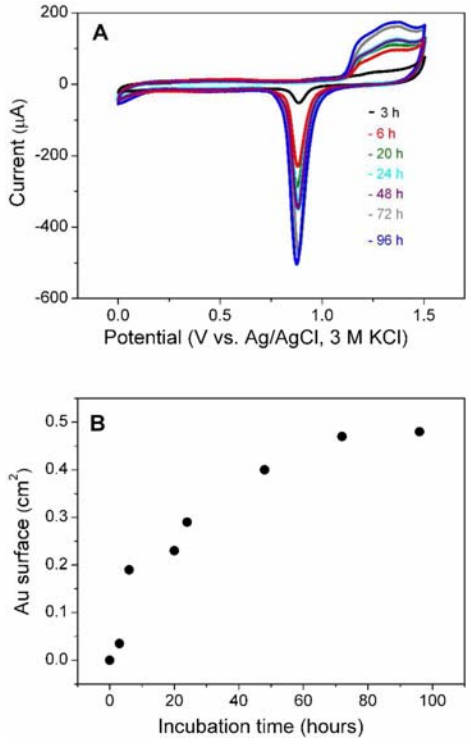


**Figure 2.** Dependence of the AuNP(5 nm) coverage on functionalized HOPG electrodes on the incubation time in the AuNP solution. (A) CVs measured at room temperature in 0.1 M $H_2SO_4$ of AuNP(5 nm)-HOPG electrodes prepared with different incubation times. Scan rate was 200 mV/s. (B) Electroactive gold surface on the AuNP(5 nm)-HOPG electrodes determined from the integration of the reduction peaks at 0.9 V of the above CVs.


dx.doi.org/10.1021/ja307308j | J. Am. Chem. Soc. 2012, 134, 17212−17220

surface of Au attached to each LDG electrode was determined by the integration of the gold oxide reduction peak, taking into account a charge of −482 $\mu$C/cm$^2$ for the reduction of a gold oxide monolayer.[23] The Au coverage results are shown in Figure 2B, indicating that a maximum of 0.47 cm$^2$ were obtained after 3 days of incubation of the modified HOPG electrode in the AuNPs solution, which is ca. 2.4 times the geometric electrode area. Taking into account the incubation time dependence of the AuNPs coverage on HOPG electrodes, the LDG electrodes were incubated in the AuNPs solution during 3 days for modification. The CVs performed in 0.1 M $H_2SO_4$ indicated that the surface of the AuNP(5 nm)-LDG electrodes covered by Au was 1.4 ± 0.4 cm$^2$, which is 20 times their geometric area (Figure S4, Supporting Information). These results suggest that a significant part of the AuNPs had been immobilized inside the pores of LDG. In the case of AuNP(16 nm)-LDG electrodes, the average Au surface measured was smaller (1.1 ± 0.1 cm$^2$), which can be explained as the larger sized AuNPs not being able to attach inside the smaller pores of LDG. As expected, the control measurement with a LDG not incubated in the AuNPs solution did not show any of the redox peaks of Au (Figure S4, Supporting Information). Control experiments by incubating nonfunctionalized LDG electrodes in the 5 nm AuNPs solution for 3 days (data not shown) were also performed. In this case, redox signals due to Au were observed, presumably due to the adsorption of AuNPs, although there was a 50−60% decrease of the detected Au after 2-day storage of the electrodes. No loss of the electrochemical signals was observed for the covalently bound AuNPs under the same conditions.

The modified AuNP(5 nm)-LDG electrodes were characterized by TEM. As it was not possible to carry out these measurements with the LDG electrodes directly, due to their size and porous structure, we scraped the surface of the electrodes and performed the TEM study on the graphite chips produced. Figure 3 shows the TEM images obtained for the graphite chips from a LDG electrode with covalently bound AuNPs and from a nonfunctionalized LDG electrode that had been incubated in AuNPs solution 3 days. The EDX analyzer indicated that the dark areas of the images correspond to Au. Much less Au is detected in the graphite chips from the nonfunctionalized LDG electrode, and the images show that the AuNPs have agglomerated together (Figure 3a−c). More Au was detected in the graphite particles produced from the AuNP(5 nm)-LDG electrodes (Figure 3d−f). In addition, the high magnification images show that many AuNPs have maintained their structure, in agreement with the size range determined spectroscopically for the AuNP suspension. Less aggregation of AuNPs is observed, which is in agreement with a covalent immobilization of the AuNPs to the functionalized LDG. As expected, no Au was detected in the samples from a nonfunctionalized LDG electrode (data not shown).

**Covalent Immobilization of *T. hirsuta* Laccase to AuNP-LDG and Electrocatalytic Properties of the Enzymatic Electrode.** To allow immobilization of *Th*Lc to the AuNP(5 nm)-LDG electrodes by covalent bonds and with the optimal orientation for DET, the attached AuNPs were functionalized. This was done by forming a mixed 4-aminophenyl and MH monolayer (Figure 1) as has been reported before for planar Au electrodes.[12c,d] First, the 4-aminophenyl groups were grafted to the AuNPs by the same method as for the LDG electrodes. The CVs performed for this modification step are shown in Figure S5 of the Supporting Information. Second, the self-assembly of MH was allowed for the Au regions not covered by the 4-aminophenyl groups. This strategy allowed optimal covalent immobilization of *Th*Lc on planar Au electrodes for DET.[12c,d] Analogously to the cited planar Au electrodes, we immobilized the *Th*Lc on the functionalized AuNP-LDG in two steps: (a) formation of imino bonds between the oxidized sugar residues of the enzyme and the amino groups of the electrode, (b) formation of amide bonds between the activated carboxylic groups of the enzyme and the amino groups of the electrode surface (Figure 1).[12c]

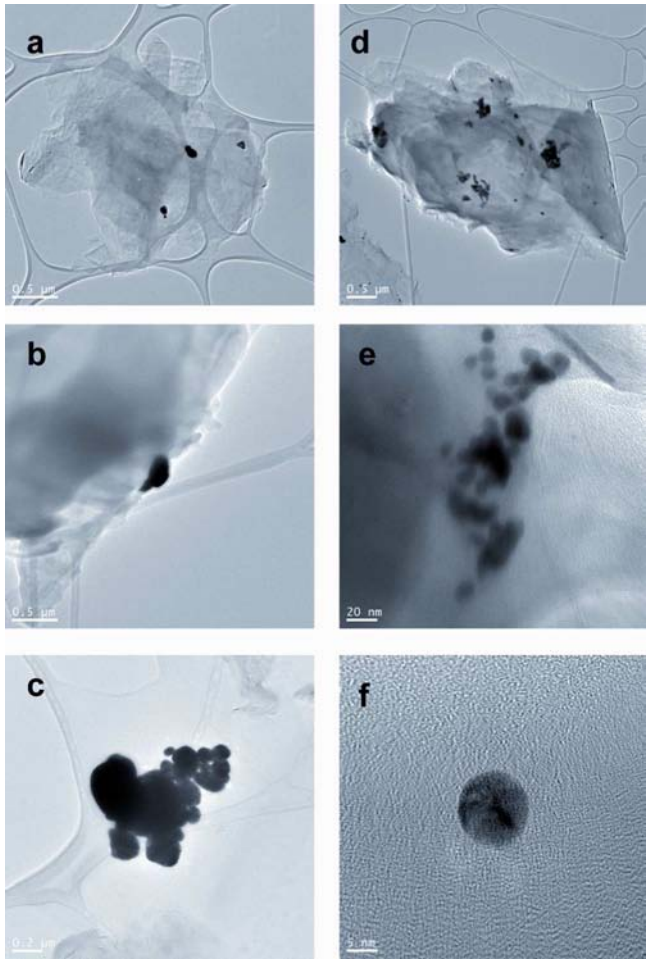


**Figure 3.** TEM images of graphite particles scraped from AuNP(5 nm)-LDG electrodes. (a−c) AuNPs of 5 nm diameter adsorbed on a LDG electrode. (d−f) AuNPs of 5 nm diameter covalently bound to a LDG electrode functionalized with 4-aminophenyl groups. Scale bars: (a), (b), and (d) 0.5 $\mu$m; (c) 0.2 $\mu$m; (e) 20 nm; (f) 5 nm.

The electrocatalytic properties of the prepared *Th*Lc-AuNP(5 nm)-LDG electrodes were evaluated by cyclic voltammetry (Figure 4). A strong reductive catalytic effect is observed in the CV that depends on the $O_2$ concentration. Rotation of the electrode at 500 rpm increased considerably the electrocatalytic current density measured compared to the stationary electrode, although further increase in the rotation rate seldom changed the CV response. Addition of NaF 30 mM, which is an enzyme inhibitor,[24] to the solution suppressed completely the electrocatalytic wave (Figure 4). Furthermore, control experiments were performed after each modification step of the electrode in the absence of laccase, in which electrocatalytic oxygen reduction at positive potentials was not observed (Figure S6, Supporting Information). Therefore, the


dx.doi.org/10.1021/ja307308j | J. Am. Chem. Soc. 2012, 134, 17212−17220

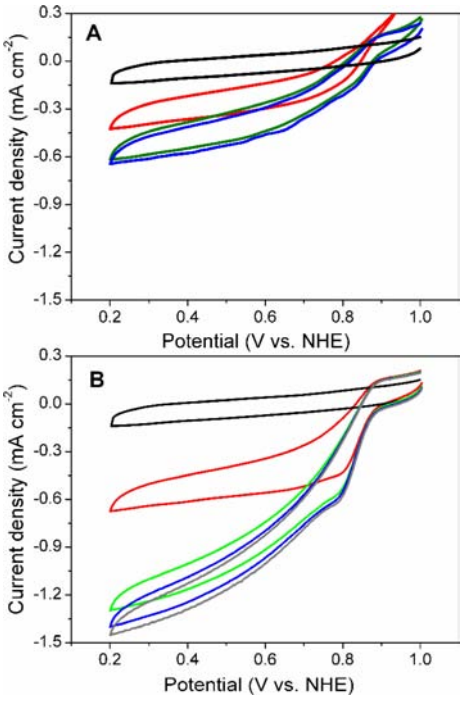


**Figure 4.** CVs of a *Th*Lc-AuNP(5 nm)-LDG electrode in 50 mM acetate buffer, pH. 4.2 with 100 mM $NaClO_4$ at 27 °C and different rotation rates under air (A) or under 1 atm $O_2$ (B). Scan rate was 10 mV/s. Rotation rates were 0 (red), 500 (green), 1000 (blue) or 1500 rpm (gray). The black line corresponds to the CV measured in presence of 30 mM NaF.

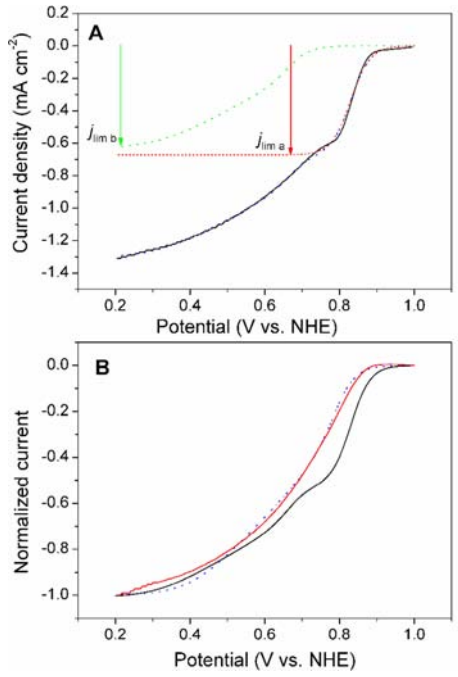


**Figure 5.** Mathematical fittings for the blank-subtracted forward scan of the CVs recorded at 1500 rpm under 1 atm of $O_2$. (A) *Th*Lc-AuNP(5 nm)-LDG electrode: Black line is the experimental CV; red dotted line is the theoretical curve of an one-electron Nernstian process with $E_a$ = 0.83 V and $j_{lim\ a}$ = −0.697 mA/cm$^2$; green dashed line is the theoretical curve for a reductive electrocatalytic process described by eq 6 of ref 25 with $E_b$ = 0.67 V, $j_{lim\ b}$ = −0.628 mA/cm$^2$, $k_{cat}/k_0^{max}$ = 0.05 and $\beta d_0$ = 9.9; blue dashed line corresponds to the addition of the red and green curves. (B) Comparison of *Th*Lc-AuNP(5 nm)-LDG and *Th*Lc-LDG electrodes: Black and red lines are the experimental CVs of *Th*Lc-AuNP(5 nm)-LDG and *Th*Lc-LDG electrodes, respectively; blue dotted line is the theoretical curve for a reductive electrocatalytic process described by eq 6 of ref 25 with $E$ = 0.79 V, $j_{lim}$ = −1.06 mA/cm$^2$, $k_{cat}/k_0^{max}$ = 0.03 and $\beta d_0$ = 11.0.

electrocatalytic reduction of $O_2$ shown in Figure 4 is due to the immobilized *Th*Lc. The electrocatalytic waves measured for all *Th*Lc-AuNP(5 nm)-LDG electrodes had a characteristic shape, which is different from those measured previously by us for *Th*Lc-Au electrodes[12c] or for *Th*Lc-LDG electrodes in absence of AuNPs (Figure S7A, Supporting Information). A biphasic kinetic behavior is observed in the CV of *Th*Lc-AuNP(5 nm)-LDG electrodes. At the higher potentials, the catalytic wave has a sigmoidal shape, whereas at the lower potentials the catalytic current gradually increases with the overpotential without reaching a real plateau. The later kinetic behavior is very similar to that observed for *Th*Lc-Au[12c] and *Th*Lc-LDG electrodes (see below).

To find an explanation for this complex kinetic behavior we subtracted the blank CV in presence of $F^-$ inhibitor to the CV measured at the higher electrode rotation rate. In this way, the capacitive current is eliminated and the dependence of the catalytic current on mass transport is very small. Then, we performed curve-fitting of the electrocatalytic forward scan. Figure 5A shows that the experimental curve can be deconvoluted into two theoretical curves. The first one (red curve, **a**) corresponds to a one-electron Nernstian process that is rate-limited by the enzymatic reaction and not by the DET between enzyme and electrode.[25] The second curve (green, **b**) corresponds to the equation developed by Leger et al. for a DET-rate limited process in which there is a superposition of different electrochemical rate constants.[25] Two parameters are determined from the fit of the sigmoidal part of the experimental curve to Nernst equation (curve **a**): the formal potential of the *Th*Lc redox center exchanging electrons with the electrode ($E_a$ = 0.83 V vs NHE) and the plateau current density ($j_{lim\ a}$ = −0.697 mA/cm$^2$). In the case of curve **b**, the corresponding parameters were $E_b$ = 0.67 V versus NHE and $j_{lim\ b}$ = −0.628 mA/cm$^2$. In addition, the fitting to curve **b** required the adjustment of two more independent parameters defined by Leger et al.: $k_{cat}/k_0^{max}$ is the ratio between the rate constants of the enzymatic reaction and of the heterogeneous electron transfer at the optimal enzyme orientation, and $\beta d_0$ accounts for the dispersion of orientations of enzyme molecules participating in DET.[25] The values of these determined parameters are given in Figure 5. In Figure 5B, the experimental electrocatalytic curve of the *Th*Lc-AuNP(5 nm)-LDG electrode is compared to that of a *Th*Lc-LDG electrode. The difference in the shape of the electrocatalytic curves is evident and very reproducible (about 10 electrodes of each type were prepared). The whole electrocatalytic curve in the absence of immobilized AuNPs can be fitted to the equation of curve **b** (Figure 5B). Typical CVs measured for a *Th*Lc-LDG electrode are shown in Figure S7A of the Supporting Information.

The influence of the immobilized AuNPs size was also studied and electrocatalytic measurements were equally performed with *Th*Lc-AuNP(16 nm)-LDG electrodes (Figure S7B, Supporting Information). In this case, the shape of the electrocatalytic wave was similar to those obtained with *Th*Lc-AuNPs(5 nm)-LDG electrodes, although the current densities measured were smaller on average (Table 1). Table 1 shows that the immobilization of AuNPs to the LDG electrodes


dx.doi.org/10.1021/ja307308j | J. Am. Chem. Soc. 2012, 134, 17212−17220

**Table 1. Catalytic Current Densities for Oxygen Reduction and Chloride Tolerance of *Th*Lc Electrodes at Different Redox Potentials versus NHE**

| electrode | $j_{0.8\ V}$ ($\mu A/cm^2$) | $j_{0.4\ V}$ ($\mu A/cm^2$) | $Cl^-$ inhibition (%)[a] |
|---|---|---|---|
| *Th*Lc-LDG | −275 ± 4 | −925 ± 15 | 0%[b]; 16%[c] |
| *Th*Lc-AuNP(5 nm)-LDG | −500 ± 10 | −1070 ± 20 | 16% |
| *Th*Lc-AuNP(16 nm)-LDG | −260 ± 10 | −820 ± 30 | 25% |
| *Th*Lc-Au[d] | −10.0 ± 0.2 | −40 ± 2 | 58%[e] |

[a]Decrease of the catalytic current at 0.4 V in presence of 140 mM $Cl^-$. [b]Data from ref 20. [c]Data from ref 13e. [d]Data from ref 12c. [e]Inhibition with 28 mM $Cl^-$.

seldom improves the electroenzymatic currents of oxygen reduction measured at high overpotentials but it does have a significant effect at low overpotentials, specially with the 5 nm ones.

Addition of ABTS to the solution, which is a typical redox mediator used for laccases, only increased 6% the catalytic current measured at 0.4 V versus NHE for a *Th*Lc-AuNPs(5 nm)-LDG electrode (Figure S8, Supporting Information). Therefore, most of the immobilized and active enzyme molecules have the adequate orientation for DET reactions.

The operational stability of the *Th*Lc-modified electrodes was studied by chronoamperometry at +0.4 V vs NHE (Figure 6). The *Th*Lc-AuNPs(5 nm)-LDG electrode was more stable

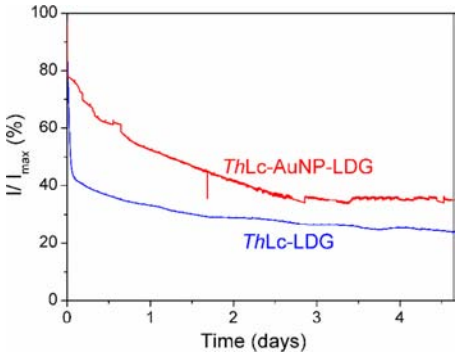


**Figure 6.** Operational stability of *Th*Lc-AuNP(5 nm)-LDG and *Th*Lc-LDG electrodes. Normalized chronoamperometry measured at an applied potential of 0.4 V vs NHE in 50 mM acetate buffer, pH 4.2, 100 mM $NaClO_4$ under 1 atm $O_2$, at 27 °C and 500 rpm electrode rotation.

under continuous operation than the *Th*Lc-LDG electrode. The *Th*Lc-LDG electrode had a strong loss of catalytic current during the first hours, probably due to diffusion of non-covalently bound enzyme molecules, which is much less pronounced for the *Th*Lc-AuNPs(5 nm)-LDG electrode. After this initial decay the catalytic currents of both types of enzyme electrodes were quite stable, retaining the *Th*Lc-AuNPs(5 nm)-LDG and the *Th*Lc-LDG electrodes 40% and 30% of the initial current, respectively.

Another important feature regarding Lc biocathodes is their resistance to $Cl^-$. $Cl^-$ is a Lc inhibitor and usually present in most human biofluids. $Cl^-$ associates to the T1 site blocking reversibly the Lc catalytic activity.[24] Covalent bonding of Lc onto electroactive surfaces[20] or incorporation of the enzyme into optimized redox hydrogels[26] yield in some cases an additional resistance to moderate concentrations of $Cl^-$. The electrochemical response to increasing NaCl additions was monitored by chronoamperometry (Figure S9 of Supporting Information). In Table 1 are expressed the values obtained for *Th*Lc-AuNP(5 nm)-LDG and *Th*Lc-AuNP(16 nm)-LDG electrodes compared with the results obtained for a *Th*Lc-Au electrode.[12c] Macroscopic Au electrodes modified with *Th*Lc have a lower $Cl^-$ resistance when compared with LDG ones; *Th*Lc-Au electrode loses 58% of its current intensity in presence of less than 30 mM $Cl^-$, while other *Th*Lc-modified graphite electrodes have shown a current decrease between 0%[20] and 16%[13e] for 140 mM $Cl^-$. In presence of 140 mM $Cl^-$, Lc-AuNPs(5 nm)-LDG and Lc-AuNPs(16 nm)-LDG electrodes showed current decreases of 16% and 25%, respectively.

## DISCUSSION

Lc-based biocathodes have been proven as a good alternative to Pt cathodes for biofuel cell applications, as these enzymes catalyze very efficiently $O_2$ electroreduction at low overpotentials.[11b] However, in order to optimize the performance of these biocathodes, several parameters need improvement. These parameters are the following: enzyme coverage on the electrode surface, rate of DET between the electrode and the enzyme redox center, and operational stability of the bioelectrode. In this work, we have addressed these issues by developing a specific strategy for *Th*Lc immobilization on a graphite electrode modified with AuNPs.

LDG shows a broad range of pore size that yields a high specific surface, and thus is an adequate platform for producing enzymatic electrodes with high biocatalyst load.[20] Up-grading the LDG electrode with AuNPs has given two additional advantages. The first one is that it allowed covering a great part of the electrode porous surface with Au (up to 20 times the geometric electrode area), which can then be tailored by surface chemistry in order to optimize the immobilized *Th*Lc orientation for DET.[12b,d] The second advantage provided by the AuNPs is their performance as electronic bridges for enhancing the rate of DET reaction between the electrode and the immobilized enzyme molecules, as has been shown by other authors for different redox enzymes.[8a−c,27]

We show that the strategy based on forming aromatic linkers by electrochemical reduction of the diazonium salt precursor for attaching both AuNPs and the laccase molecules to the electrode leads to a biocathode with a high operational stability. This high stability can be attributed to the covalent immobilization of the enzyme, decreasing its leakage from the electrode, but also to the formation of stable C−Au bonds between the AuNPs and the LDG electrodes. The formation of covalent C−Au bonds on the surface of AuNPs has been demonstrated by SERS[21b] and XPS[14,22] characterization. Furthermore, our TEM images have shown that covalent bonding of the AuNPs to the graphite electrode increases the structural integrity of the former compared to the adsorption modification method.

The high electrocatalytic currents of $O_2$ reduction measured for *Th*Lc-AuNP-LDG electrodes in DET mode can be attributed to the oriented immobilization of the enzyme with the CuT1 site facing the nanostructured surface. The *Th*Lc immobilization was performed by a strategy previously developed by us for planar Au electrodes.. This strategy is based on the formation of a mixed functional layer of 4-aminophenyl and MH groups onto the Au surface for the two-step covalent immobilization of the enzyme. Electrocatalytical measurements and other results by different surface character-


dx.doi.org/10.1021/ja307308j | J. Am. Chem. Soc. 2012, 134, 17212−17220

ization techniques showed that this strategy favored oriented immobilization of *Th*Lc.[12c,d] Accordingly, the addition of the redox mediator ABTS to the solution hardly increased the electrocatalytic current of *Th*Lc-AuNP(5 nm)-LDG electrodes, whereas we have reported previously that the mediated catalytic current was twice higher the DET-based one for the same *Th*Lc covalently bound to LDG electrodes through amide bonds only.[20] Moreover, the effect of redox mediator addition was even smaller for the *Th*Lc-AuNPs(5 nm)-LDG electrode than for *Th*Lc-Au electrode (a 6% increase for the former compared to a 20% increase of the later).[12c] Therefore, the nanometric dimensions of the AuNPs provides an extra enhancement of the immobilized enzyme DET reaction rate.

This enhancement of DET is clearly visible in the shape of the electrocatalytic wave measured by cyclic voltammetry. The bioelectrocatalytic wave of the CVs can be deconvoluted in two contributions. The first one is centered at 0.83 V and corresponds to a bioelectrocatalytic process with very fast DET kinetics. This redox potential value ($E_a$) is near to the formal redox potential of the T1 Cu site of *Th*Lc determined by spectroelectrochemistry ($E_{T1}$ = 0.78 V).[15] Besides, this fast DET process was not observed in the absence of AuNPs immobilized on the electrode nor in a previous work in which *Th*Lc was immobilized on planar Au.[12c] These results suggest that this part of the electrocatalytic wave corresponds to *Th*Lc molecules optimally connected to the AuNPs via their Cu T1 site. It has been reported in several works that AuNPs can enhance the rate of DET between immobilized redox proteins and electrodes. Jensen et al. reported that the long-range DET of cytochrome *c* increased by more of 1 order of magnitude when 3−4 nm AuNPs were intercalated between the protein and a Au(111) electrode.[27] Even glucose oxidase, which has its FAD redox center buried within the protein structure, can achieve fast DET when immobilized with the correct orientation on 1.4 nm diameter AuNPs.[8a,c] Therefore, the very fast DET-based electrocatalytic currents measured in the present work can be attributed to the efficient electronic coupling between the Cu T1 sites of the *Th*Lc molecules and the functionalized 5 nm AuNPs of the electrode surface due to the oriented immobilization strategy followed.

The second contribution to the electrocatalytic waves measured with the *Th*Lc-AuNP-LDG electrodes can be fitted to a DET-rate limited process in which there is a superposition of different electrochemical rate constants.[25] The value of the formal potential determined for the redox center involved in this process is $E_b$ = 0.67 V, which is approximately ca. 100 mV lower than that of the Cu T1 site.[15] However, $E_b$ is too high to be attributed to the Cu T2/T3 site ($E_{T2/T3}$ = 0.4 V).[28] Besides, the curve fitting of this part of the electrocatalytic curve requires adjusting three more parameters. Thus, the individual values of the parameters determined should be taken carefully in this case. In fact, reasonable fits could be obtained by fixing $E_b$ at higher values, although not at the $E_{T2}$ value. On the other hand, we cannot rule out that the $E_{T1}$ value could be affected in some extent by covalent binding of the enzyme to the electrode surface. Abad et al. reported that the formal potential of the Cu center of galactose oxidase changed approximately 100 mV, when the enzyme was specifically attached via this Cu site to AuNPs.[8b] Taking into account that the electrocatalytic waves measured with *Th*Lc-LDG electrodes could be fitted completely to the DET-rate limited process with similar parameters of $\beta d_o$, and $k_{cat}/k_0^{max}$, it is probable that in the case of *Th*Lc-AuNP-LDG electrodes the second contribution of the electrocatalytic wave corresponds to enzyme molecules covalently bound to functional groups of the LDG surface instead to those of the AuNPs. As the LDG electrode surface is very porous, it is reasonable to think that not all accessible areas of the electrode were covered by the AuNPs.

Recently has been published a deep study of the bioelectrocatalytic properties of two bilirubin oxidases (BOx), which are also MCOs, adsorbed on graphite electrodes.[29] Two successive catalytic waves were also observed for the Box-modified carbon electrodes, in all likelihood due to two different orientations of the enzyme on the electrode surface, with either the CuT1 site or the CuT2/T3 in DET contact.[29] However, this is not the case for *Th*Lc-based electrodes, fabricated and studied in the present work, because only the electrocatalytic wave due to the CuT1 site ($E_a \approx E_{T1}$ for *Th*Lc-LDG electrodes) is observed in absence of AuNPs. Furthermore, the second contribution to the electrocatalytic wave of *Th*Lc-AuNP-LDG electrodes starts at potentials much higher than that of the low redox potential intermediate of the CuT2/T3 site of MCOs, as stated above. This difference in electrocatalytic behavior between the two enzymatic electrodes is attributed to the immobilization mode of the enzyme (oriented covalent binding vs random adsorption) rather than to the type of MCO. This statement is supported by the experimental result shown in Figure S8 (Supporting Information), where the addition of the mediator ABTS supposed a current increase of only a 6%. As most of the enzymes are oriented with its T1 site facing the electrode, the fraction for a hypothetical electrocatalytic current starting from the T2/T3 Cu site is not appreciated in the electrocatalytic process (Figure 4). In fact, when in a previous work *Th*Lc was randomly adsorbed onto Au electrodes, two electrocatalytic currents of $O_2$ reduction were measured at the redox potentials of the Cu T1 and Cu T2/T3 sites.[28]

The limiting current density ($j_{lim}$) when a bioelectrocatalytic reaction is rate-determined by the enzymatic reaction is:[30]

$$j_{lim} = \frac{nF\Gamma k_{cat} C}{C + K_M} \quad (1)$$

Here $n$ is the number of electrons involved in the electrocatalytic process, $F$ is the Faraday constant, $\Gamma$ is the enzyme coverage on the electrode, $k_{cat}$ is the turnover number of the enzyme, $C$ is the substrate concentration and $K_M$ is the Michaelis−Menten constant of the enzymatic reaction. Therefore, the two plateau currents ($j_{lim\ a}$ and $j_{lim\ b}$) estimated from the deconvolution of the electrocatalytic wave of Figure 5 are proportional to the two populations of immobilized *Th*Lc that perform DET: those that are efficiently wired to the electrode via the AuNPs ($\Gamma_a$) and those that have slower rate of DET ($\Gamma_b$). Assuming that the enzymatic parameters $k_{cat}$ and $K_M$ are the same for all active immobilized *Th*Lc molecules because they are covalently bound by the same way, we can estimate that $\Gamma_a$ and $\Gamma_b$ correspond to 53% and 47% of the total *Th*Lc coverage, respectively. For other *Th*Lc-AuNP(5 nm)-LDG electrodes, this ratio was also similar (around 50% for each enzyme population).

The value of $k_{cat}$ of the immobilized laccase is unknown, but we did measure this value for the enzyme in solution using ABTS as electron donor, 397 $s^{-1}$. From this value, we can estimate that the $k_{cat}$ for the active *Th*Lc molecules bound to the electrodes is ≥397 $s^{-1}$ because their catalytic turnover does not include the step of electron exchange with ABTS. In the

case of the efficiently wired laccase molecules via the AuNPs, the electroenzymatic process is not rate-limited by DET. The measured current at each potential is dependent only on the enzymatic turnover and on the amount of laccase molecules with the Cu T1 site reduced according to Nernst equilibrium. This means that the heterogeneous electron transfer rate constant ($k_o$) for the *Th*Lc molecules efficiently wired via the AuNPs is much larger than $k_{cat}$.[25] Thus, we can estimate that in that case $k_o \gg 397\ s^{-1}$, which is much larger than those measured by Laviron's method[31] for redox enzymes wired to electrodes using AuNPs. Xiao et al. reported $k_o$ values up to 88 $s^{-1}$ for glucose oxidase wired via FAD-modified AuNPs,[8a] whereas smaller values around 0.5−1 $s^{-1}$ have been measured for copper metalloenzymes, such as galactose oxidase[8b] and the same *Th*Lc used in the present work. In the latter case, the enzyme was directly adsorbed onto 50 nm AuNP layers deposited onto a Au electrode; thus, the *Th*Lc/AuNPs/ electrode integration was very different to the one reported in the present work.[13a] Besides, the determination of the $k_o$ of enzymes immobilized on electrodes by Laviron's method is based on the peak-separation dependence on the scan rate of the noncatalytic redox signal measured by cyclic voltammetry.[31] To measure these noncatalytic redox signal, a high coverage of immobilized enzyme molecules is required,[32] and molecules with different orientations will contribute to the DET, some of which maybe even due to catalytically inactive ones. This will make broader the redox waves measured and decrease the determined $k_0$. On the contrary, in our electrocatalytic results we are able to differentiate the contribution of the enzyme molecules that are efficiently wired to the electrode via the AuNPs from those which DET is rate-limiting the electrocatalytic process. Therefore, we can conclude that when laccase molecules are adequately connected to AuNPs by a specific and oriented immobilization strategy their $k_0$ becomes much higher than their catalytic turnover, leading to very fast DET at low overpotentials.

The electrocatalytic results obtained with the immobilized 16 nm-diameter AuNPs were not as good as the ones measured with the 5 nm-diameter ones. The decrease of the electrocatalytic current density at high overpotentials of the former is proportional to the decrease of their coverage on the LDG surface, as they are not able to modify the smaller pores of the electrode. However, the decrease of the electrocatalytic current density with 16 nm AuNPs at low overpotential is much more evident, approximately 50% of that measured with 5 nm AuNPs. Therefore, the size of the AuNPs must affect the electronic coupling of *Th*Lc molecules. This suggests that the 5 nm AuNPs, whose size is comparable to that of the *Th*Lc molecules,[33] are able to interact more closely with the Cu T1 site cavity of the enzyme, accelerating DET. A similar effect has been described by El-Deab et al. for the coupling of another copper enzyme, superoxide dismutase, and AuNPs of different shapes and sizes. Those AuNPs enriched in Au(100) orientation with a projection morphology favored the DET reaction of superoxide dismutase.[34]

It has been shown in previous works that macroscopic gold surfaces are not suitable for avoiding $Cl^-$ inhibition drawback, whereas carbon-based electrodes are.[13e,20] This effect might be caused by a $Cl^-$ preconcentration effect that occurs by the anions adsorption on gold. The use of AuNPs instead of macroscopic Au surfaces limits the presence of free gold surface, mitigating the $Cl^-$ inhibition caused by gold massive surfaces. Measurements carried on in this work show that the AuNPs(5 nm) seldom contribute to $Cl^-$ inhibition increase of the *Th*Lc electrode when compared with nanostructured graphite electrodes,[13e] but including AuNPs(16 nm) does lead to a significant increase in $Cl^-$ sensitivity. This result might suggest that the smaller AuNPs, which are of comparable size to *Th*Lc and can be inserted in the smaller pores of the LDG, present much less Au surface available for $Cl^-$ adsorption or association with positively charged aminophenyl groups exposed to the surface. The larger AuNPs, on the contrary, will present more of their surface exposed to $Cl^-$ adsorption even if they are modified by one or more *Th*Lc molecules.

## ■ CONCLUSIONS AND PERSPECTIVES

The results presented here show the preparation and characterization of a stable nanostructured laccase electrode based on step-by-step covalent attachment of AuNPs and *Th*Lc to porous graphite electrodes using the diazonium salt electrochemical reduction strategy. Oriented immobilization of the redox enzyme on adequately functionalized AuNPs allows establishing very fast DET with the electrode via their Cu T1 site. Therefore, in this way *Th*Lc electrodes can be prepared that produce high electrocatalytic current densities of oxygen reduction at very low overpotentials, such as −0.5 mA/ $m^2$ at 0.8 V versus NHE. The efficient electronic coupling between *Th*Lc and AuNPs depends not only on the adequate orientation of the immobilized enzyme molecules, but also on the size of the AuNPs, obtaining best results when the AuNPs have similar dimensions to those of *Th*Lc (approximately 5 nm diameter). Additionally, the use of the correct amount of Au mitigates undesirable effects like chloride inhibition. Our results show that the electrocatalytic waves measured with the *Th*Lc-AuNP-LDG electrodes can be deconvoluted into two contributions. The one at the lower overpotentials corresponds to immobilized enzyme molecules that are efficiently wired by the AuNPs, with a heterogeneous electron transfer rate of $k_0 \gg 400\ s^{-1}$. The contribution at higher overpotentials corresponds to immobilized enzyme molecules less efficiently wired to the electrode, so that the bioelectrocatalytic process is rate-limited by a DET reaction with a distribution of $k_0$ values.

**Abbreviations.** ABTS, 2,2′-azinobis-(3-ethylbenzothiazoline-6-sulfonic acid) diammonium salt; AuNPs, gold nanoparticles; CV, cyclic voltammogram; DET, direct electron transfer; EDC, 1-(3-dimethylaminopropyl)-3-ethylcarbodiimide; *Th*Lc, *Trametes hirsuta* laccase; LDG, low density graphite; MET, mediated electron transfer; MCO, multicopper oxidase; MH, 6-mercapto-1-hexanol; NHS, *N*-hydroxysuccinimide; THPC, tetrakis(hydroxymethyl)phosphonium chloride.

## ■ ASSOCIATED CONTENT

### Supporting Information

Hg porosimetry characterization of LDG electrodes, CVs of the modification of LDG and AuNP-LDG electrodes, electrocatalytic reduction of $O_2$ by *Th*Lc-LDG and *Th*Lc-AuNP(16 nm)-LDG electrodes, mediated electrocatalytic reduction of $O_2$ by *Th*Lc-AuNP(5 nm)-LDG electrode, controls CVs in the absence of laccase, inhibition of electrocatalysis by halides. This material is available free of charge via the Internet at http://pubs.acs.org.

## ■ AUTHOR INFORMATION

### Corresponding Author

marcospita@icp.csic.es; alopez@icp.csic.es

**Present Address**
[§]Instituto de Química Física "Rocasolano", CSIC, E-28006, Madrid, Spain.

**Notes**
The authors declare no competing financial interest.

## ■ ACKNOWLEDGMENTS

This work was funded by the European Research Council, project 3D-NanoBioDevice NMP4-SL-2009-229255 and the Spanish MICINN, project CTQ2009-12649. M.P. acknowledges the Ramon y Cajal 2009 program from the Spanish MINECO and C.V.-D. acknowledges a JAE-Doc fellowship from CSIC. We thank Mr. Ramón Tomé for skillful technical aid.

## ■ REFERENCES

(1) Bartlett, P. N. *Bioelectrochemistry: Fundamentals, Experimental Techniques and Applications*; John Wiley & Sons Ltd: West Sussex, U.K., 2008.
(2) (a) Katz, E.; Willner, I. *Electroanalysis* **2003**, *15*, 913−947. (b) Wang, J. *Electroanalysis* **2001**, *13*, 983−988. (c) Kumlanghan, A.; Liu, J.; Thavarungkul, P.; Kanatharana, P.; Mattiasson, B. *Biosens. Bioelectron.* **2007**, *22*, 2939−2944.
(3) Aulenta, F.; Catervi, A.; Majone, M.; Panero, S.; Reale, P.; Rossetti, S. *Environ. Sci. Technol.* **2007**, *41*, 2554−2559.
(4) (a) Barton, S. C.; Gallaway, J.; Atanassov, P. *Chem. Rev.* **2004**, *104*, 4867−4886. (b) Katz, E.; Pita, M. *Chem.—Eur. J.* **2009**, *15*, 12554−12564.
(5) (a) Cracknell, J. A.; Vincent, K. A.; Armstrong, F. A. *Chem. Rev.* **2008**, *108*, 2439−2461. (b) Leger, C.; Bertrand, P. *Chem. Rev.* **2008**, *108*, 2379−2438.
(6) (a) Schuhmann, W. *Biosensors Bioelectron.* **1995**, *10*, 181−193. (b) De Lacey, A. L.; Detcheverry, M.; Moiroux, J.; Bourdillon, C. *Biotechnol. Bioeng.* **2000**, *68*, 1−10. (c) Morozov, S. V.; Karyakina, E. E.; Zorin, N. A.; Varfolomeyev, S. D.; Cosnier, S.; Karyakin, A. A. *Bioelectrochemistry* **2002**, *55*, 169−171. (d) Mao, F.; Mano, N.; Heller, A. *J. Am. Chem. Soc.* **2003**, *125*, 4951−4957.
(7) (a) Fantuzzi, A.; Fairhead, M.; Gilardi, G. *J. Am. Chem. Soc.* **2004**, *126*, 5040−5041. (b) Rüdiger, O.; Abad, J. M.; Hatchikian, E. C.; Fernandez, V. M.; De Lacey, A. L.. *J. Am. Chem. Soc.* **2005**, *127*, 16008−16009. (c) Stoica, L.; Dimcheva, N.; Haltrich, D.; Ruzgas, T.; Gorton, L. *Biosens. Bioelectron.* **2005**, *20*, 2010−2018. (d) Blanford, C. F.; Heath, R. S.; Armstrong, F. A. *Chem. Commun.* **2007**, 1710−1712.
(8) (a) Xiao, Y.; Patolsky, F.; Katz, E.; Hainfeld, J. F.; Willner, I. *Science* **2003**, *299*, 1877−1881. (b) Abad, J. M.; Gass, M.; Bleloch, A.; Schiffrin, D. J. *J. Am. Chem. Soc.* **2009**, *131*, 10229−10236. (c) Holland, J. T.; Lau, C.; Brozik, S.; Atanassov, P.; Banta, S. *J. Am. Chem. Soc.* **2011**, *133*, 19262−19265. (d) Miyake, T.; Yoshino, S.; Yamada, T.; Hata, K.; Nishizawa, M. *J. Am. Chem. Soc.* **2011**, *133*, 5129−5134.
(9) (a) Alonso-Lomillo, M. A.; Rüdiger, O.; Maroto-Valiente, A.; Velez, M.; Rodriguez-Ramos, I.; Muñoz, F. J.; Fernandez, V. M.; De Lacey, A. L. *Nano Lett.* **2007**, *7*, 1603−1608. (b) Murata, K.; Kajiya, K.; Nakamura, N.; Ohno, H. *Energy Environ. Sci.* **2009**, *2*, 1280−1285. (c) Salaj-Kosla, U.; Poller, S.; Beyl, Y.; Scanlon, M. D.; Beloshapkin, S.; Shleev, S.; Schuhmann, W.; Magner, E. *Electrochem. Commun.* **2012**, *16*, 92−95.
(10) (a) Shleev, S.; Tkac, J.; Christenson, A.; Ruzgas, T.; Yaropolov, A. I; Whittaker, J. W.; Gorton, L. *Biosens. Bioelectron.* **2005**, *20*, 2517−2554. (b) Solomon, E. I.; Augustine, A. J..; Yoon, J. *Dalton Trans.* **2008**, 3921−3932.
(11) (a) Barton, S. C.; Kim, H. H.; Binyamin, G.; Zhang, Y.; Heller, A. *J. Am. Chem. Soc.* **2001**, *123*, 5802−5803. (b) Soukharev, V.; Mano, N.; Heller, A. *J. Am. Chem. Soc.* **2004**, *126*, 8368−8369. (c) Ackermann, Y.; Guschin, D. A.; Eckhard, K.; Shleev, S.; Schuhmann, W. *Electrochem. Commun.* **2010**, *12*, 640−643. (d) Rengaraj, S.; Mani, V.; Kavanagh, P.; Rusling, J.; Leech, D. *Chem. Commun.* **2011**, *47*, 11861−11863.
(12) (a) Blanford, C. F.; Foster, C. E.; Heath, R. S.; Armstrong, F. A. *Faraday Discuss.* **2008**, *140*, 319−335. (b) Thorum, M. S.; Anderson, C. A.; Hatch, J. J.; Campbell, A. S.; Marshall, N. M.; Zimmerman, S. C.; Lu, Y.; Gewirth, A. A. *J. Phys. Chem. Lett.* **2010**, *1*, 2251−2254. (c) Pita, M.; Gutierrez-Sanchez, C.; Olea, D.; Velez, M.; Garcia-Diego, C.; Shleev, S.; Fernandez, V. M.; De Lacey, A. L. *J. Phys. Chem. C.* **2011**, *115*, 13420−13428. (d) Vaz-Dominguez, C.; Pita, M.; de Lacey, A. L.; Shleev, S.; Cuesta, A. *J. Phys. Chem. C.* **2012**, *116*, 16532−16540.
(13) (a) Dagys, M.; Haberska, K.; Shleev, S.; Arnebrant, T.; Kulys, J.; Ruzgas, T. *Electrochem. Commun.* **2010**, *12*, 933−935. (b) Miyake, T.; Yoshino, S.; Yamada, T.; Hata, K.; Nishizawa, M. *J. Am. Chem. Soc.* **2011**, *133*, 5129−5134. (c) Meredith, M. T.; Minson, M.; Hickey, D.; Artyushkova, K.; Glatzhofer, D. T.; Minteer, S. D. *ACS Catal.* **2011**, *1*, 1683−1690. (d) Luckarift, H. R.; Ivnitski, D. M.; Lau, C.; Kriipin, C.; Atanassov, P.; Johnson, G. R. *Electroanalysis* **2012**, *24*, 931−937. (e) Gutierrez-Sanchez., C.; Jia, W.; Beyl, Y.; Pita., M.; Schuhmann, W.; De Lacey, A. L.; Stoica, L. *Electrochim. Acta* **2012**, *82*, 218−223.
(14) Liu, G.; Luais, E.; Gooding, J. J. *Langmuir* **2011**, *27*, 4176−4183.
(15) Shleev, S.; Morozova, O. V.; Nikitina, V. O.; Gorshina, E. S.; Rusinova, T. V.; Serezhenkov, V. A.; Burbaev, D. S.; Gazaryan, I. G.; Yaropolov, A. I. *Biochimie* **2004**, *86*, 693−703.
(16) Bradford, M. M. *Anal. Biochem.* **1976**, *72*, 248−254.
(17) Duff, D. G.; Baiker, A.; Edwards, P. P. *Langmuir* **1993**, *9*, 2301−2309.
(18) Frens, G. *Nat. Phys. Sci.* **1973**, *241*, 20−22.
(19) Haiss, W.; Thanh, N. T. K.; Aveyard, J.; Fernig, D. G. *Anal. Chem.* **2007**, *79*, 4215−4221.
(20) Vaz-Dominguez, C.; Campuzano, S.; Rüdiger, O.; Pita, M.; Gorbacheva, M.; Shleev, S.; Fernandez, V. M.; De Lacey, A. L. *Biosens. Bioelectron.* **2008**, *24*, 531−537.
(21) (a) Lehr, J.; Williamson, B. E.; Flavel, B. S.; Downard, A. J. *Langmuir* **2009**, *25*, 13503−13509. (b) Laurentius, L.; Stoyanov, S. R.; Gusarov, S.; Kovalenko, A.; Du, R.; Lopinski, G. P.; McDermott, M. T. *ACS Nano* **2011**, *5*, 4219−4227.
(22) Mirkhalaf, F.; Schiffrin, D. J. *Langmuir* **2010**, *26*, 14995−15001.
(23) Oesch, U.; Janata, J. *Electrochim. Acta* **1983**, *28*, 1237−1246.
(24) (a) Naki, A.; Varfolomeev, S. D. *Biochemistry (Moscow)* **1981**, *46*, 1344−1350. (b) Xu, F.; Berka, R. M.; Wahleithner, J. A.; Nelson, B. A.; Shuster, J. R.; Brown, S. H.; Palmer, A. E.; Solomon, E. I. *Biochem. J.* **1998**, *334*, 63−70.
(25) Leger, C.; Jones, A. K.; Albracht, S. P. J.; Armstrong, F. A. *J. Phys. Chem. B* **2002**, *106*, 13058−13063.
(26) Beyl, Y.; Guschin, D. A.; Shleev, S.; Schuhmann, W. *Electrochem. Commun.* **2011**, *13*, 474−476.
(27) Jensen, P. S.; Chi, Q.; Grumsen, F. B.; Abad, J. M.; Horsewell, A.; Schiffrin, D. J.; Ulstrup, J. *J. Phys. Chem. C* **2007**, *111*, 6124−6132.
(28) Shleev, S.; Pita, M.; Yaropolov, A. I.; Ruzgas, T.; Gorton, L. *Electroanalysis* **2006**, *18*, 1901−1908.
(29) Shleev, S.; Andoralov, V.; Falk, M.; Reimann, C. T.; Ruzgas, T.; Srnec, M.; Ryde, U.; Rulisek, L. *Electroanalysis* **2012**, *24*, 1524−1540.
(30) Sucheta, A.; Cammack, R.; Weiner, J.; Armstrong, F. A. *Biochemistry* **1993**, *32*, 5455−5465.
(31) Laviron, E. *J. Electroanal. Chem.* **1979**, *101*, 19−28.
(32) Pershad, H. R.; Duff, J. L. C.; Heering, H. A.; Duin, E. C.; Albracht, S. P. J.; Armstrong, F. A. *Biochemistry* **1999**, *38*, 8992−8999.
(33) Polyakov, K. M.; Federova, T. V.; Stepanova, E. V.; Cherkashin, E. A.; Kurzeev, S. A; Strokopytov, B. V.; Lamzin, V. S.; Koroleva, O. V. *Acta Crystallogr.* **2009**, *65*, 611−617.
(34) El-Deab, M. S.; Ohsaka, T. *Electrochem. Commun.* **2007**, *9*, 641−656.